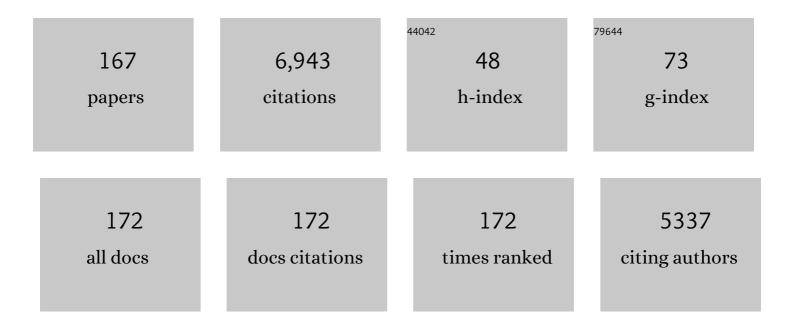
Zuotai Zhang

List of Publications by Year in descending order

Source: https://exaly.com/author-pdf/4110067/publications.pdf Version: 2024-02-01



#	Article	lF	CITATIONS
1	Metal–organic framework-derived magnetic carbon for efficient decontamination of organic pollutants via periodate activation: Surface atomic structure and mechanistic considerations. Journal of Hazardous Materials, 2022, 424, 126786.	6.5	38
2	lonization potential-based design of deep eutectic solvent for recycling of spent lithium ion batteries. Chemical Engineering Journal, 2022, 436, 133200.	6.6	38
3	Future trend of terminal energy conservation in steelmaking plant: Integration of molten slag heat recovery-combustible gas preparation from waste plastics and CO2 emission reduction. Energy, 2022, 239, 122543.	4.5	13
4	Bowknot-like Zr/La bimetallic organic frameworks for enhanced arsenate and phosphate removal: Combined experimental and DFT studies. Journal of Colloid and Interface Science, 2022, 614, 47-57.	5.0	20
5	The effect of soil amendment derived from P-enhanced sludge pyrochar on ryegrass growth and soil microbial diversity. Science of the Total Environment, 2022, 813, 152526.	3.9	9
6	Amine-functionalized nano-Al2O3 adsorbent for CO2 separation from biogas: Efficient CO2 uptake and high anti-urea stability. Journal of Cleaner Production, 2022, 332, 130078.	4.6	18
7	Decarbonising the iron and steel sector for a 2 °C target using inherent waste streams. Nature Communications, 2022, 13, 297.	5.8	26
8	Emission levels and phase distributions of PCDD/Fs in a full-scale municipal solid waste incinerator: The impact of wet scrubber system. Journal of Cleaner Production, 2022, 337, 130468.	4.6	14
9	Remarkably enhanced photocatalytic performance of Au/AgNbO3 heterostructures by coupling piezotronic with plasmonic effects. Nano Energy, 2022, 95, 107031.	8.2	51
10	Electric potential-determined redox intermediates for effective recycling of spent lithium-ion batteries. Green Chemistry, 2022, 24, 3723-3735.	4.6	10
11	In situ synthesis of Tree-branch-like Copper-manganese oxides nanoarrays supported on copper foam as a superior efficiency Fenton-like catalyst for enhanced degradation of 4-chlorophenol. Applied Surface Science, 2022, 593, 153241.	3.1	12
12	Harvesting mechanical energy for hydrogen generation by piezoelectric metal–organic frameworks. Materials Horizons, 2022, 9, 1978-1983.	6.4	20
13	Sulfur-containing iron nanocomposites confined in S/N co-doped carbon for catalytic peroxymonosulfate oxidation of organic pollutants: Low iron leaching, degradation mechanism and intermediates. Chemical Engineering Journal, 2021, 404, 126499.	6.6	77
14	Synergic removal of tetracycline using hydrophilic three-dimensional nitrogen-doped porous carbon embedded with copper oxide nanoparticles by coupling adsorption and photocatalytic oxidation processes. Journal of Colloid and Interface Science, 2021, 581, 350-361.	5.0	23
15	Highly efficient and stable PEI@Al2O3 adsorbents derived from coal fly ash for biogas upgrading. Chemical Engineering Journal, 2021, 409, 128117.	6.6	24
16	Enhanced and environment-friendly chemical looping gasification of crop straw using red mud as a sinter-resistant oxygen carrier. Waste Management, 2021, 121, 354-364.	3.7	43
17	Enhanced Piezocatalytic Activity of Sr _{0.5} Ba _{0.5} Nb ₂ O ₆ Nanostructures by Engineering Surface Oxygen Vacancies and Self-Generated Heterojunctions. ACS Applied Materials & Interfaces, 2021, 13, 7259-7267.	4.0	45
18	Biogas Upgrading via Cyclic CO ₂ Adsorption: Application of Highly Regenerable PEI@nano-Al ₂ O ₃ Adsorbents with Anti-Urea Properties. Environmental Science & Technology, 2021, 55, 5236-5247.	4.6	42

#	Article	IF	CITATIONS
19	Remediation of Cu-polluted soil with analcime synthesized from engineering abandoned soils through green chemistry approaches. Journal of Hazardous Materials, 2021, 406, 124673.	6.5	11
20	Atomically Dispersed Cobalt Sites on Graphene as Efficient Periodate Activators for Selective Organic Pollutant Degradation. Environmental Science & amp; Technology, 2021, 55, 5357-5370.	4.6	149
21	Performance and mechanism of mold-pressing alkali-activated material from MSWI fly ash for its heavy metals solidification. Waste Management, 2021, 126, 747-753.	3.7	20
22	Cobaltâ€Enhanced Mass Transfer and Catalytic Production of Sulfate Radicals in MOFâ€Derived CeO ₂ • Co ₃ O ₄ Nanoflowers for Efficient Degradation of Antibiotics. Small, 2021, 17, e2101393.	5.2	28
23	Enhancement of Scattering and Near Field of TiO ₂ –Au Nanohybrids Using a Silver Resonator for Efficient Plasmonic Photocatalysis. ACS Applied Materials & Interfaces, 2021, 13, 34714-34723.	4.0	27
24	Efficient conversion of carbohydrates and biomass into furan compounds by chitin/Ag co-modified H3PW12O40 catalysts. Journal of Cleaner Production, 2021, 316, 128243.	4.6	12
25	Ce-based heterogeneous catalysts by partial thermal decomposition of Ce-MOFs in activation of peroxymonosulfate for the removal of organic pollutants under visible light. Chemosphere, 2021, 280, 130637.	4.2	30
26	Regulation of electronic structures of MOF-derived carbon via ligand adjustment for enhanced Fenton-like reactions. Science of the Total Environment, 2021, 799, 149497.	3.9	20
27	A green synthesis of PEI@nano-SiO ₂ adsorbent from coal fly ash: selective and efficient CO ₂ adsorption from biogas. Sustainable Energy and Fuels, 2021, 5, 1014-1025.	2.5	13
28	Fabrication of Pd/CeO ₂ nanocubes as highly efficient catalysts for degradation of formaldehyde at room temperature. Catalysis Science and Technology, 2021, 11, 6732-6741.	2.1	12
29	Feasibility Evaluation of the Terminated Waste Energy In Situ Conversion Strategy toward Carbon Neutralization in Metallurgical Processes. ACS Sustainable Chemistry and Engineering, 2021, 9, 14079-14089.	3.2	8
30	Efficient one-pot synthesis of ethyl levulinate from carbohydrates catalyzed by Wells-Dawson heteropolyacid supported on Ce–Si pillared montmorillonite. Journal of Cleaner Production, 2021, 324, 129276.	4.6	9
31	An all-in-one strategy for the adsorption of heavy metal ions and photodegradation of organic pollutants using steel slag-derived calcium silicate hydrate. Journal of Hazardous Materials, 2020, 382, 121120.	6.5	75
32	Levels, spatial distribution, and source identification of airborne environmentally persistent free radicals from tree leaves. Environmental Pollution, 2020, 257, 113353.	3.7	15
33	Reduction-ammoniacal leaching to recycle lithium, cobalt, and nickel from spent lithium-ion batteries with a hydrothermal method: Effect of reductants and ammonium salts. Waste Management, 2020, 102, 122-130.	3.7	64
34	Efficient recovery of phosphorus in sewage sludge through hydroxylapatite enhancement formation aided by calcium-based additives. Water Research, 2020, 171, 115450.	5.3	46
35	Defective analcime/geopolymer composite membrane derived from fly ash for ultrafast and highly efficient filtration of organic pollutants. Journal of Hazardous Materials, 2020, 388, 121736.	6.5	34
36	Pollution emission characteristics, distribution of heavy metals, and particle morphologies in a hazardous waste incinerator processing phenolic waste. Journal of Hazardous Materials, 2020, 388, 121751.	6.5	23

#	Article	IF	CITATIONS
37	Recycling of spent lithium-ion batteries: Selective ammonia leaching of valuable metals and simultaneous synthesis of high-purity manganese carbonate. Waste Management, 2020, 114, 253-262.	3.7	54
38	All-inorganic dual-phase halide perovskite nanorings. Nano Research, 2020, 13, 2994-3000.	5.8	18
39	Evolution of trace elements and polluting gases toward clean co-combustion of coal and sewage sludge. Fuel, 2020, 280, 118685.	3.4	25
40	COVID-19 waste management: Effective and successful measures in Wuhan, China. Resources, Conservation and Recycling, 2020, 163, 105071.	5.3	132
41	Cross-sectoral synergy between municipal wastewater treatment, cement manufacture and petrochemical synthesis via clean transformation of sewage sludge. Sustainable Energy and Fuels, 2020, 4, 6274-6282.	2.5	4
42	Exclusive enhancement of catalytic activity in Bi _{0.5} Na _{0.5} TiO ₃ nanostructures: new insights into the design of efficient piezocatalysts and piezo-photocatalysts. Journal of Materials Chemistry A, 2020, 8, 16238-16245.	5.2	93
43	PCDD/F levels and phase distributions in a full-scale municipal solid waste incinerator with co-incinerating sewage sludge. Waste Management, 2020, 106, 110-119.	3.7	41
44	Microwave-assisted hydrothermal assembly of 2D copper-porphyrin metal-organic frameworks for the removal of dyes and antibiotics from water. Environmental Science and Pollution Research, 2020, 27, 39186-39197.	2.7	54
45	Novel Recovered Compound Phosphate Fertilizer Produced from Sewage Sludge and Its Incinerated Ash. ACS Sustainable Chemistry and Engineering, 2020, 8, 6611-6621.	3.2	21
46	Recent Advances of Ferro-, Piezo-, and Pyroelectric Nanomaterials for Catalytic Applications. ACS Applied Nano Materials, 2020, 3, 1063-1079.	2.4	205
47	Colloidal Co single-atom catalyst: a facile synthesis strategy and high catalytic activity for hydrogen generation. Green Chemistry, 2020, 22, 1269-1274.	4.6	15
48	A novel method for screening deep eutectic solvent to recycle the cathode of Li-ion batteries. Green Chemistry, 2020, 22, 4473-4482.	4.6	158
49	Self-templated microwave-assisted hydrothermal synthesis of two-dimensional holey hydroxyapatite nanosheets for efficient heavy metal removal. Environmental Science and Pollution Research, 2019, 26, 30076-30086.	2.7	25
50	Investigation of formation mechanism of particulate matter in a laboratory-scale simulated cement kiln co-processing municipal sewage sludge. Journal of Cleaner Production, 2019, 234, 822-831.	4.6	15
51	Epitaxial patterned Bi ₂ FeCrO ₆ nanoisland arrays with room temperature multiferroic properties. Nanoscale Advances, 2019, 1, 2139-2145.	2.2	6
52	Coordination-Directed Assembly of Luminescent Semiconducting Oligomers and Weak Interaction-Induced Morphology Transformation. ACS Omega, 2019, 4, 14294-14300.	1.6	5
53	Few-layer transition metal dichalcogenides (MoS2, WS2, and WSe2) for water splitting and degradation of organic pollutants: Understanding the piezocatalytic effect. Nano Energy, 2019, 66, 104083.	8.2	181
54	Enhanced catalytic performance by multi-field coupling in KNbO3 nanostructures: Piezo-photocatalytic and ferro-photoelectrochemical effects. Nano Energy, 2019, 58, 695-705.	8.2	240

#	Article	IF	CITATIONS
55	Luffa sponge-derived hierarchical meso/macroporous boron nitride fibers as superior sorbents for heavy metal sequestration. Journal of Hazardous Materials, 2019, 378, 120669.	6.5	26
56	A field study of polychlorinated dibenzo-p-dioxins and dibenzofurans formation mechanism in a hazardous waste incinerator: Emission reduction strategies. Journal of Cleaner Production, 2019, 232, 1018-1027.	4.6	38
57	Amino-functionalized sewage sludge-derived biochar as sustainable efficient adsorbent for Cu(II) removal. Waste Management, 2019, 90, 17-28.	3.7	72
58	Role of SnS ₂ in 2D–2D SnS ₂ /TiO ₂ Nanosheet Heterojunctions for Photocatalytic Hydrogen Evolution. ACS Applied Nano Materials, 2019, 2, 2144-2151.	2.4	69
59	Calcium-looping reforming of methane realizes in situ CO ₂ utilization with improved energy efficiency. Science Advances, 2019, 5, eaav5077.	4.7	153
60	In Situ Study on the Transformation Behavior of Ti-Bearing Slags in the Oxidation Atmosphere. Minerals, Metals and Materials Series, 2019, , 51-59.	0.3	0
61	Copper-nanoparticle-dispersed amorphous BaTiO ₃ thin films as hole-trapping centers: enhanced photocatalytic activity and stability. RSC Advances, 2019, 9, 5045-5052.	1.7	6
62	Surface-disorder-engineered Zn2SnO4/SnO2 hollow microboxes with enhanced solar-driven photocatalytic activity. Applied Surface Science, 2019, 463, 474-480.	3.1	19
63	TiO2/CuS heterostructure nanowire array photoanodes toward water oxidation: The role of CuS. Applied Surface Science, 2019, 463, 829-837.	3.1	37
64	Biomass gasification using the waste heat from high temperature slags in a mixture of CO2 and H2O. Energy, 2019, 167, 688-697.	4.5	28
65	General roles of sludge ash, CaO and Al2O3 on the sludge pyrolysis toward clean utilizations. Applied Energy, 2019, 233-234, 412-423.	5.1	29
66	Integrating biomass pyrolysis with waste heat recovery from hot slags via extending the C-loops: Product yields and roles of slags. Energy, 2018, 149, 792-803.	4.5	23
67	Application of washed MSWI fly ash in cement composites: long-term environmental impacts. Environmental Science and Pollution Research, 2018, 25, 12127-12138.	2.7	29
68	Distributional and compositional insight into the polluting materials during sludge combustion: Roles of ash. Fuel, 2018, 220, 318-329.	3.4	10
69	Phosphorus speciation in sewage sludge and the sludge-derived biochar by a combination of experimental methods and theoretical simulation. Water Research, 2018, 140, 90-99.	5.3	69
70	Understanding the Relationship Between Structure and Thermophysical Properties of CaO-SiO2-MgO-Al2O3 Molten Slags. Metallurgical and Materials Transactions B: Process Metallurgy and Materials Processing Science, 2018, 49, 677-687.	1.0	51
71	Recycling of municipal solid waste incineration by-product for cement composites preparation. Construction and Building Materials, 2018, 162, 794-801.	3.2	84
72	Data processing to support explication about effect of mineral constituents on temperature-dependent structural characterization of carbon fractions in sewage sludge-derived biochar. Data in Brief, 2018, 17, 1304-1306.	0.5	5

#	Article	IF	CITATIONS
73	Utilization of High-Temperature Slags From Metallurgy Based on Crystallization Behaviors. Jom, 2018, 70, 1274-1281.	0.9	6
74	Product characteristics and kinetics of sewage sludge pyrolysis driven by alkaline earth metals. Energy, 2018, 153, 921-932.	4.5	51
75	Characterization of PM10 surrounding a cement plant with integrated facilities for co-processing of hazardous wastes. Journal of Cleaner Production, 2018, 186, 831-839.	4.6	18
76	Effect of mineral constituents on temperature-dependent structural characterization of carbon fractions in sewage sludge-derived biochar. Journal of Cleaner Production, 2018, 172, 3342-3350.	4.6	63
77	Rational design of a novel quaternary ZnO@ZnS/Ag@Ag ₂ S nanojunction system for enhanced photocatalytic H ₂ production. Inorganic Chemistry Frontiers, 2018, 5, 3074-3081.	3.0	21
78	Template-Free Synthesis of Oxygen-Doped Bundlelike Porous Boron Nitride for Highly Efficient Removal of Heavy Metals from Wastewater. ACS Sustainable Chemistry and Engineering, 2018, 6, 16011-16020.	3.2	43
79	Inherent potential of steelmaking to contribute to decarbonisation targets via industrial carbon capture and storage. Nature Communications, 2018, 9, 4422.	5.8	78
80	Hierarchically Structured Calcium Silicate Hydrate-Based Nanocomposites Derived from Steel Slag for Highly Efficient Heavy Metal Removal from Wastewater. ACS Sustainable Chemistry and Engineering, 2018, 6, 14926-14935.	3.2	94
81	Effect of inherent minerals on sewage sludge pyrolysis: Product characteristics, kinetics and thermodynamics. Waste Management, 2018, 80, 175-185.	3.7	53
82	Alkali metal-driven release behaviors of volatiles during sewage sludge pyrolysis. Journal of Cleaner Production, 2018, 203, 860-872.	4.6	34
83	MOF-Derived Porous ZnO Nanocages/rGO/Carbon Sponge-Based Photocatalytic Microreactor for Efficient Degradation of Water Pollutants and Hydrogen Evolution. ACS Sustainable Chemistry and Engineering, 2018, 6, 11989-11998.	3.2	101
84	PAHs and heavy metals in the surrounding soil of a cement plant Co-Processing hazardous waste. Chemosphere, 2018, 210, 247-256.	4.2	47
85	Recycling ground MSWI bottom ash in cement composites: Long-term environmental impacts. Waste Management, 2018, 78, 841-848.	3.7	46
86	Morphology-tunable tellurium nanomaterials produced by the tellurite-reducing bacterium Lysinibacillus sp. ZYM-1. Environmental Science and Pollution Research, 2018, 25, 20756-20768.	2.7	13
87	Long-term leaching behaviours of cement composites prepared by hazardous wastes. RSC Advances, 2018, 8, 27602-27609.	1.7	5
88	Cellular and compositional insight into the sludge dewatering process using enzyme treatment. Environmental Science and Pollution Research, 2018, 25, 28942-28953.	2.7	11
89	Novel Calcium Oxide-Enhancement Phosphorus Recycling Technique through Sewage Sludge Pyrolysis. ACS Sustainable Chemistry and Engineering, 2018, 6, 9167-9177.	3.2	41
90	Environmental mitigation of sludge combustion via two opposite modifying strategies: Kinetics and stabilization effect. Fuel, 2018, 227, 346-354.	3.4	13

#	Article	IF	CITATIONS
91	Structural Investigation of Phosphorus in CaO-SiO2-P2O5 Ternary Glass. Metallurgical and Materials Transactions B: Process Metallurgy and Materials Processing Science, 2017, 48, 1139-1148.	1.0	21
92	Integrated Utilization of Sewage Sludge for the Cement Clinker Production. Minerals, Metals and Materials Series, 2017, , 95-102.	0.3	1
93	Effect of Calcium Hydroxide on the Pyrolysis Behavior of Sewage Sludge: Reaction Characteristics and Kinetics. Energy & amp; Fuels, 2017, 31, 5079-5087.	2.5	30
94	Simulating the effects of anchors on the thermal performance of building insulation systems. Energy and Buildings, 2017, 140, 501-507.	3.1	23
95	Effect of water-washing on the co-removal of chlorine and heavy metals in air pollution control residue from MSW incineration. Waste Management, 2017, 68, 221-231.	3.7	62
96	Investigation on Viscosity and Nonisothermal Crystallization Behavior of P-Bearing Steelmaking Slags with Varying TiO2 Content. Metallurgical and Materials Transactions B: Process Metallurgy and Materials Processing Science, 2017, 48, 527-537.	1.0	28
97	Energy Saving and Emission Reduction from the Steel Industry: Heat Recovery from High Temperature Slags. Lecture Notes in Energy, 2017, , 249-280.	0.2	1
98	Role of steel slags on biomass/carbon dioxide gasification integrated with recovery of high temperature heat. Bioresource Technology, 2017, 223, 1-9.	4.8	21
99	Effect of TiO2 on Thermophysical Properties and Structure of P-Bearing Steelmaking Slags. Minerals, Metals and Materials Series, 2017, , 411-418.	0.3	1
100	Short-range and Medium-range Structural Order in CaO–SiO ₂ –TiO ₂ –B ₂ O _{3 Glasses. ISIJ International, 2016, 56, 752-758.}	&l t)/ s ub&ş	jt;32
101	Viscous Flow and Crystallization Behaviors of P-bearing Steelmaking Slags with Varying Fluorine Content. ISIJ International, 2016, 56, 546-553.	0.6	12
102	Integrated Utilization of Sewage Sludge and Coal Gangue for Cement Clinker Products: Promoting Tricalcium Silicate Formation and Trace Elements Immobilization. Materials, 2016, 9, 275.	1.3	17
103	Preparation of novel ceramic tiles with high Al2O3 content derived from coal fly ash. Construction and Building Materials, 2016, 114, 888-895.	3.2	69
104	Integrated biomass gasification using the waste heat from hot slags: Control of syngas and polluting gas releases. Energy, 2016, 114, 165-176.	4.5	17
105	A Fe-C-Ca big cycle in modern carbon-intensive industries: toward emission reduction and resource utilization. Scientific Reports, 2016, 6, 22323.	1.6	6
106	The partitioning behavior of trace element and its distribution in the surrounding soil of a cement plant integrated utilization of hazardous wastes. Environmental Science and Pollution Research, 2016, 23, 13943-13953.	2.7	7
107	Integration of biomass/steam gasification with heat recovery from hot slags: Thermodynamic characteristics. International Journal of Hydrogen Energy, 2016, 41, 5916-5926.	3.8	24
108	Modification of the Structure of Ti-Bearing Mold Flux by the Simultaneous Addition of B2O3 and Na2O. Metallurgical and Materials Transactions E, 2016, 3, 28-36.	0.5	4

#	Article	IF	CITATIONS
109	Disposal of High-Temperature Slags: A Review of Integration of Heat Recovery and Material Recycling. Metallurgical and Materials Transactions E, 2016, 3, 114-122.	0.5	3
110	Effect of Al2O3 Addition on the Precipitated Phase Transformation in Ti-Bearing Blast Furnace Slags. Metallurgical and Materials Transactions B: Process Metallurgy and Materials Processing Science, 2016, 47, 1390-1399.	1.0	21
111	In situ DRIFTS studies on MnO nanowires supported by activated semi-coke for low temperature selective catalytic reduction of NO with NH3. Applied Surface Science, 2016, 366, 139-147.	3.1	71
112	Environmental investigation on co-combustion of sewage sludge and coal gangue: SO 2 , NO x and trace elements emissions. Waste Management, 2016, 50, 213-221.	3.7	108
113	Oxidation behavior of β-SiAlON powders fabricated by combustion synthesis. Ceramics International, 2016, 42, 7290-7299.	2.3	12
114	Preparation of glass ceramic foams for thermal insulation applications from coal fly ash and waste glass. Construction and Building Materials, 2016, 112, 398-405.	3.2	211
115	Heat Recovery from High Temperature Slags: Chemical Methods. , 2016, , 41-48.		2
116	Viscous and Crystallization Characteristics of CaO-SiO2-MgO-Al2O3-FetO-P2O5-(CaF2) Steelmaking Slags. , 2016, , 495-500.		0
117	Integration of coal gasification and waste heat recovery from high temperature steel slags: an emerging strategy to emission reduction. Scientific Reports, 2015, 5, 16591.	1.6	19
118	Oxidation of Ca-α-SiAlON Powders Prepared by Combustion Synthesis. Materials, 2015, 8, 7549-7562.	1.3	2
119	Facile and Economical Preparation of SiAlON-Based Composites Using Coal Gangue: From Fundamental to Industrial Application. Energies, 2015, 8, 7428-7440.	1.6	9
120	Co-modification and Crystalline-control of Ti-bearing Blast Furnace Slags. ISIJ International, 2015, 55, 158-165.	0.6	25
121	Enhancement of Rutile Formation by ZrO ₂ Addition in Ti-bearing Blast Furnace Slags. ISIJ International, 2015, 55, 1384-1389.	0.6	7
122	Preparation and modeling of energy-saving building materials by using industrial solid waste. Energy and Buildings, 2015, 97, 6-12.	3.1	10
123	Integrated carbon dioxide/sludge gasification using waste heat from hot slags: Syngas production and sulfur dioxide fixation. Bioresource Technology, 2015, 181, 174-182.	4.8	53
124	Investigation on slag fiber characteristics: Mechanical property and anti-corrosion performance. Ceramics International, 2015, 41, 5677-5687.	2.3	20
125	Promoting effect of Nd on the reduction of NO with NH ₃ over CeO ₂ supported by activated semi-coke: an in situ DRIFTS study. Catalysis Science and Technology, 2015, 5, 2251-2259.	2.1	105
126	Co-combustion and emission characteristics of coal gangue and low-quality coal. Journal of Thermal Analysis and Calorimetry, 2015, 120, 1883-1892.	2.0	31

#	Article	IF	CITATIONS
127	Effect of Al2O3 on the Viscosity and Structure of CaO-SiO2-MgO-Al2O3-FetO Slags. Metallurgical and Materials Transactions B: Process Metallurgy and Materials Processing Science, 2015, 46, 537-541.	1.0	65
128	A Novel Kinematic Model for Molten Slag Fiberization: Prediction of Slag Fiber Properties. Metallurgical and Materials Transactions B: Process Metallurgy and Materials Processing Science, 2015, 46, 993-1001.	1.0	12
129	Selective Crystallization Behavior of CaO-SiO2-Al2O3-MgO-FetO-P2O5 Steelmaking Slags Modified through P2O5 and Al2O3. Metallurgical and Materials Transactions B: Process Metallurgy and Materials Processing Science, 2015, 46, 2246-2254.	1.0	33
130	Achieving waste to energy through sewage sludge gasification using hot slags: syngas production. Scientific Reports, 2015, 5, 11436.	1.6	27
131	Heat Recovery from High Temperature Slags: A Review of Chemical Methods. Energies, 2015, 8, 1917-1935.	1.6	83
132	Synthesis, characterization and modeling of new building insulation material using ceramic polishing waste residue. Construction and Building Materials, 2015, 85, 119-126.	3.2	63
133	Fuel nitrogen conversion and release of nitrogen oxides during coal gangue calcination. Environmental Science and Pollution Research, 2015, 22, 7139-7146.	2.7	23
134	FTIR, Raman and NMR investigation of CaO–SiO2–P2O5 and CaO–SiO2–TiO2–P2O5 glasses. Journal c Non-Crystalline Solids, 2015, 420, 26-33.	of 1.5	102
135	Facile and economical synthesis of porous activated semi-cokes for highly efficient and fast removal of microcystin-LR. Journal of Hazardous Materials, 2015, 299, 325-332.	6.5	17
136	Trace element partitioning behavior of coal gangue-fired CFB plant: experimental and equilibrium calculation. Environmental Science and Pollution Research, 2015, 22, 15469-15478.	2.7	29
137	Structural Roles of Boron and Silicon in the CaO-SiO2-B2O3 Glasses Using FTIR, Raman, and NMR Spectroscopy. Metallurgical and Materials Transactions B: Process Metallurgy and Materials Processing Science, 2015, 46, 1549-1554.	1.0	62
138	Two-stage high temperature sludge gasification using the waste heat from hot blast furnace slags. Bioresource Technology, 2015, 198, 364-371.	4.8	45
139	Thermodynamic modeling of electrolyte solutions by a hybrid ion-interaction and solvation (HIS) model. Calphad: Computer Coupling of Phase Diagrams and Thermochemistry, 2015, 48, 79-88.	0.7	5
140	Effects of chemistry and mineral on structural evolution and chemical reactivity of coal gangue during calcination: towards efficient utilization. Materials and Structures/Materiaux Et Constructions, 2015, 48, 2779-2793.	1.3	48
141	Thermophysical Properties of Modified Ti-bearing Blast Furnace Slags. , 2015, , 703-709.		0
142	Effect of P2O5 Addition on the Viscosity and Structure of Titanium Bearing Blast Furnace Slags. ISIJ International, 2014, 54, 1491-1497.	0.6	23
143	Effect of B2O3 on the Structure and Viscous Behavior of Ti-Bearing Blast Furnace Slags. Jom, 2014, 66, 2168-2175.	0.9	55
144	Multi-Stage Control of Waste Heat Recovery from High Temperature Slags Based on Time Temperature Transformation Curves. Energies, 2014, 7, 1673-1684.	1.6	42

#	Article	IF	CITATIONS
145	Preparation of Slag Wool by Integrated Waste-Heat Recovery and Resource Recycling of Molten Blast Furnace Slags: From Fundamental to Industrial Application. Energies, 2014, 7, 3121-3135.	1.6	40
146	Characteristics of low temperature biomass gasification and syngas release behavior using hot slag. RSC Advances, 2014, 4, 62105-62114.	1.7	36
147	Pyrite transformation and sulfur dioxide release during calcination of coal gangue. RSC Advances, 2014, 4, 42506-42513.	1.7	27
148	Experimental investigation and modeling of cooling processes of high temperature slags. Energy, 2014, 76, 761-767.	4.5	61
149	Development of the random simulation model for estimating the effective thermal conductivity of insulation materials. Building and Environment, 2014, 80, 221-227.	3.0	21
150	In situ DRIFTS investigation on the SCR of NO with NH3 over V2O5 catalyst supported by activated semi-coke. Applied Surface Science, 2014, 313, 660-669.	3.1	145
151	Investigation of the Viscosity and Structural Properties of CaO-SiO2-TiO2 Slags. Metallurgical and Materials Transactions B: Process Metallurgy and Materials Processing Science, 2014, 45, 1389-1397.	1.0	99
152	The Effect of P2O5 on the Crystallization Behaviors of Ti-Bearing Blast Furnace Slags Using Single Hot Thermocouple Technique. Metallurgical and Materials Transactions B: Process Metallurgy and Materials Processing Science, 2014, 45, 1446-1455.	1.0	40
153	Low-temperature SCR of NO with NH3 over activated semi-coke composite-supported rare earth oxides. Applied Surface Science, 2014, 309, 1-10.	3.1	71
154	Oxidation kinetics of magnesium aluminum oxynitride–boron nitride (MgAlON–BN) composites. Journal of the Ceramic Society of Japan, 2014, 122, 829-834.	0.5	0
155	Raman spectroscopic study of the structural properties of CaO–MgO–SiO2–TiO2 slags. Journal of Non-Crystalline Solids, 2013, 376, 209-215.	1.5	79
156	Activated Semi-coke in SO ₂ Removal from Flue Gas: Selection of Activation Methodology and Desulfurization Mechanism Study. Energy & amp; Fuels, 2013, 27, 3080-3089.	2.5	78
157	Influence of Basicity and TiO2 Content on the Precipitation Behavior of the Ti-bearing Blast Furnace Slags. ISIJ International, 2013, 53, 1696-1703.	0.6	50
158	Molecular Dynamics Study of the Structural Properties of Calcium Aluminosilicate Slags with Varying Al2O3/SiO2 Ratios. ISIJ International, 2012, 52, 342-349.	0.6	92
159	Hydrothermal Synthesis of CeO ₂ Nanoparticles on Activated Carbon with Enhanced Desulfurization Activity. Energy & Fuels, 2012, 26, 5879-5886.	2.5	45
160	Effect of Al ₂ 0 ₃ /SiO ₂ Ratio on the Viscosity and Structure of Slags. ISIJ International, 2012, 52, 753-758.	0.6	90
161	Crystallization Behavior of Rutile in the Synthesized Ti-bearing Blast Furnace Slag Using Single Hot Thermocouple Technique. ISIJ International, 2011, 51, 1396-1402.	0.6	58
162	The Influence of SiO ₂ on the Extraction of Ti Element from Tiâ€bearing Blast Furnace Slag. Steel Research International, 2011, 82, 607-614.	1.0	55

#	Article	IF	CITATIONS
163	Thermal Expansion of Magnesium Aluminum Oxynitride (Mg0.1Al1.6O2.2N0.2). High Temperature Materials and Processes, 2008, 27, .	0.6	2
164	The Influence of Al ₂ O ₃ /SiO ₂ Ratio on the Viscosity of Mold Fluxes. ISIJ International, 2008, 48, 739-746.	0.6	83
165	Synthesis and characterization of MgAlON–BN composites. International Journal of Materials Research, 2007, 98, 64-71.	0.1	3
166	Mechanical properties and microstructures of hot-pressed MgAlON–BN composites. Journal of the European Ceramic Society, 2007, 27, 319-326.	2.8	40
167	Kinetic studies of oxidation of γ-AlON–TiN composites. Journal of Alloys and Compounds, 2005, 387, 74-81.	2.8	12